

Visualizing the Variability of Gradients in Uncertain 2D Scalar Fields

Tobias Pfaffelmoser, Mihaela Mihai and Rüdiger Westermann

Abstract—In uncertain scalar fields where data values vary with a certain probability, the strength of this variability indicates the confidence in the data. It does not, however, allow inferring on the effect of uncertainty on differential quantities such as the gradient, which depend on the variability of the rate of change of the data. Analyzing the variability of the gradient is nonetheless more complicated, since, unlike scalars, gradients vary in both strength and direction, requiring initially the mathematical derivation of their respective multivariate distributions, and then the development of effective analysis techniques for these distributions.

This paper takes a first step into this direction: Based on the stochastic modeling of uncertainty via multivariate Gaussian distributions, we start by deriving uncertainty parameters, such as the mean and the covariance matrix, for gradients in uncertain discrete scalar fields. Then, for the first time to our best knowledge, we develop a mathematical framework for computing probability distributions for both the gradient orientation and the strength of the derivative in the mean gradient direction. While this framework generalizes to 3D uncertain scalar fields, we concentrate on the visualization of the resulting distributions in 2D fields. We propose a novel color mapping scheme using diffusion to visualize the variability of the derivative strength, and we introduce a special family of circular glyphs to convey the orientation distribution of uncertain vector quantities. For a number of synthetic and real-world data sets, we demonstrate the use of our approach for analyzing the stability of iso-contours in uncertain 2D scalar fields, with respect to both position and orientation. We further discuss possibilities to extend these visualization techniques to 3D and emphasize problems that arise in higher dimensions.

Index Terms—Uncertainty visualization, gradient variability, structural uncertainty, glyphs.



1 INTRODUCTION

IN an uncertain scalar field where each probability density function of data values at a certain spatial point can be approximated by a Gaussian probability density function, standard deviations are primary indicators for the degree of variation of these values. Thus, standard deviations are a means to classify the confidence in the data values, and, to this purpose, are often visualized directly, for instance, via confidence regions, uncertainty glyphs, or specific color or opacity mappings [1], [2].

The standard deviation, nonetheless, is of limited use for a rigorous analysis of uncertain data, because it does not allow inferring on the *relative variability* of data values at different points. This means, in particular, that the effect of uncertainty on differential quantities, which depend on the rate of change of the data, cannot be analyzed. Such quantities, however, play a major role in data analysis, to indicate the location and orientation of important geometric features, such as object boundaries or iso-contours.

In this work, we analyze the effect of uncertainty on the variability of gradients in scalar fields, with respect to both magnitude and orientation. Such an investigation helps answer primary questions on the stability of features in scalar fields. For instance, if a feature classifier depends on the gradient magnitude and a point has been classified as belonging to the feature, a low variability of the gradient magnitude indicates with a high level of certainty the point's membership to the feature. Then, a low variability in gradient orientation shows that the shape of the iso-contour passing through the respective spatial point is very likely to remain unchanged, even if the standard deviation shows a high

spread in the data values. On the contrary, a high uncertainty in gradient orientation indicates a likely change in the orientation of the contour, even though a low standard deviation might be observed.

Assessing the variability of gradients can therefore reveal the stability of features and their geometric structures in scalar fields. It is, however, considerably more complicated than determining the data variability via the standard deviation, because no stochastic model describing the spread in magnitude and orientation is available initially. Thus, one first has to derive the random distributions of both quantities analytically, before effective analysis techniques for these distributions can be developed.

This paper takes a first step into this direction: Based on the stochastic modeling of uncertainty via multivariate Gaussian distributions, we first derive uncertainty parameters, such as the mean and the covariance matrix, for gradients in uncertain scalar fields. The Gaussian distribution serves as a placeholder for the more general class of uni-modal distribution functions that can be characterized by the parameters mean and standard deviation. Using Gaussian distributions to model uncertainty stochastically is prevalent in the field of uncertainty visualization, although so far Gaussian distributions have mostly been used to model the local uncertainty, which can be completely characterized by the standard deviations. Our work is thus a natural extension that strives for an analysis of the effects of uncertainty on derived quantities that depend on data values at more than one spatial point. Multi-modal distributions, on the other hand, for which means and standard deviations do not serve as reliable characteristic parameters, would require first an adequate stochastic model to visualize the uncertainty of the data values themselves, before going further to analyze possible effects on differential quantities like gradients.

Building upon uncertainty parameters, we then develop a mathematical framework to analytically derive probability distributions

• T. Pfaffelmoser, M. Mihai and R. Westermann are with the Computer Graphics and Visualization Group, Technische Universität München, Informatik 15, Boltzmannstrasse 3, 85748 Garching, Germany.
E-Mail: {pfaffelmoser,mihaela.mihai,westermann}@tum.de

for both the gradient orientation and the strength of the derivative in the mean gradient direction. To the best of our knowledge, this is the first time that analytic expressions for such distributions in uncertain scalar fields have been derived. Separating the derivative strength from the gradient orientation gives rise to an effective analysis of the gradient uncertainty with respect to slope, as well as orientation. The resulting framework generalizes to 3D uncertain scalar fields, but, due to page limitations, in this paper we only provide the mathematical derivation in 2D. The 3D case is discussed in a technical report available online at [3].

Our ultimate goal is to develop visualization techniques to qualitatively assess the gradient variability in uncertain 2D scalar fields. This is challenging, because both the data values and the gradients' probability distributions need to be represented graphically in one single view. We address this issue by separately visualizing the distribution of the derivative strength and the orientation distribution. For the first case, we introduce a novel color mapping scheme involving color diffusion. The fundamental idea is to continually diffuse the colors of a base pattern, revealing the distribution of data values in the initial field, with preselected colors representing different degrees of uncertainty. By controlling the diffusion strength via the degree of derivative uncertainty, a clear differentiation between geometric features of high and low stability is obtained. For the second case, we propose a special family of circular glyphs, where a glyph's pattern and color convey the spread in direction and the uncertainty degree, respectively. We also sketch possible extensions of these methods to 3D, although, due to the inherent occlusions in 3D, some more specifically tailored techniques are required.

In summary, the particular contributions of our paper are:

- A derivation of uncertainty parameters like the mean and covariance for gradients in uncertain scalar fields given on discrete grid structures.
- Analytic expressions of the probability distributions describing the gradients' magnitude and orientation variability in Gaussian distributed uncertain scalar fields.
- A visualization technique using color diffusion to indicate the stability of the slope along the gradient direction in 2D scalar fields.
- A family of patterned and colored glyphs to quantitatively depict the uncertainty in the orientation of iso-contours in 2D scalar fields.

To validate our techniques, we apply them to visualize the gradient uncertainty in a number of data sets. We use a synthetic data set to illustrate how our approaches convey additional information that cannot be obtained from the mean values and standard deviations alone. In several real-world data sets we further confirm the strength of our approaches to analyze important geometric features with respect to their possible changes due to uncertainty.

The remainder of the paper is as follows: In the next section we discuss previous work that is related to ours. Next, we derive the uncertainty parameters for gradients in uncertain scalar fields, given on discrete grids. Then, we introduce stochastic models for the gradient variability in magnitude and orientation. Two methods for visualizing the gradient uncertainty are proposed in section 4, starting with the visualization of the derivative uncertainty in the mean gradient direction, and then addressing the visualization of the variability of the gradient orientation. Results and a discussion of the relevance and usefulness of our approaches are given in the following section. We conclude the paper with an overview of the contributions and some remarks on future work and challenges for an adaption to 3D.

2 RELATED WORK

Uncertainty visualization has been acknowledged as one of the principal research topics in visualization for more than a decade now [2], yet the visual indication of uncertainties in scientific data sets is still far from standard. Most of the efforts in this area have been restricted to particular fields, such as geographical information systems [4], seismology [5], and astrophysics [6], to give just a few examples. An overview and taxonomy of uncertainty visualization techniques is given in [1], [7], [8]. The web-library at [9] provides a list of references to the major publications in the field.

One method to represent uncertainty is overloading, whereby uncertainty is treated as secondary data that is visualized in addition to the primary data. Here, the standard deviation from a given mean value is often visualized directly via specific color and opacity mappings, animations, texture, glyphs, or additional surface structures [10], [11], [12], [13], [14]. Although such approaches can provide a good indication of the local uncertainty strength, inferring how the position and structure of specific features in the data are affected by the uncertainty is nonetheless difficult.

Alternative techniques visually encode the positional variation that is caused by the uncertainty on specific features, for instance, the positional variability of surfaces in space. Methods include the visualization of confidence surfaces [2], [15] and flowlines [16], surface diffusion techniques [17], as well as surface animations [18]. The most recent approaches [19], [20], [21] model the uncertainty stochastically and derive probability distributions for particular stochastic events associated to iso-surfaces. [22] and [23] give qualitative insight into possible structural variations of salient features in scalar fields, by visualizing positive and inverse global and local correlation structures in uncertain Gaussian distributed 2D and 3D scalar fields. Then, [24] puts forward a numerical technique to show locally the covariance and cross-covariance fields of a 2D stochastic simulation. As far as we are aware of, however, none of these techniques allows quantitative inferring on the stability of structural properties of particular features in the data.

This kind of insight into the variability of features can be obtained by going beyond uncertainty indicators like the mean and the variance, and analyzing derived quantities, such as gradients. In the context of feature variability as treated in this paper, examining gradients is appealing because these quantities pertain to the uncertainty at multiple values in the data, rather than just at one local position. On the contrary, methods proposed up to this moment have mainly considered uncertainty given by a scalar value, e.g., the standard deviation. To our best knowledge, no such investigations addressing the variability of gradients in uncertain scalar fields have been performed so far.

Nevertheless, several visualization techniques have been developed to represent uncertainty in magnitude and orientation of the individual vectors in vector fields generally. Different glyph techniques are presented in [25], where the authors experiment with various arrow glyphs that use the width of the arrow head to indicate uni-modal angular uncertainty and additional arrow heads for the range of possible magnitudes. Rectangular glyphs, together with additional less emphasized lines to encode the uncertainty, are used for bidirectional vector fields in [26]. The applicability of the approach is nonetheless limited to the chosen scalar geological model parameters, which are approximated to follow a Gaussian distribution.

In the tractography domain, [27] introduces a so-called "cone

of uncertainty” 3D glyphs to visualize the orientation and corresponding uncertainty of brain fibers. The directional information is approximated by the principal eigenvector of the diffusion tensor, while the associated uncertainty, stemming from noise in MR images, is estimated via bootstrap methods. [28] combines patterns with glyphs to map an anisotropic reaction-diffusion model to vector magnitude and orientation, by producing spot patterns of various shapes, sizes, orientations, and densities, where uncertainty in orientation can be qualitatively incorporated in the amount of anisotropy that gives the shape of the spot.

[29] uses cross-advection and error diffusion in a texture-based flow visualization, where uncertainty in flow direction arising during data acquisition is revealed by changing the spatial frequency orthogonal to the flow direction. A modified LIC approach is presented in [30], to convey uncertainty in 2D steady flow fields. Here, the magnitude and direction of vector fields are taken to be described by presumably existent probability density functions. Probabilistic numerical integration in uncertain vector fields is also performed in [31], [32], where the vector fields are assumed to be Gaussian distributed. The normal distribution supposition, however, does not extend to the vector magnitude and orientation, and no distinction is made between the two quantities. Furthermore, like all other approaches based on numerical integration, the method suffers from the accumulation of errors during integration. In [33], the local distribution functions of uncertain vector quantities are computed via Monte Carlo sampling, the stochastic properties being derived from a set of realizations of the uncertain vector data via a computationally expensive process. These methods differ from our approach, in that we analyze the variability of vectors locally via an analytical mathematical derivation of the probability density functions. Moreover, we distinguish between vector magnitude and orientation, rather than combine the two in one representation.

3 GRADIENT UNCERTAINTY

This section introduces the mathematical foundations necessary to define gradients in a scalar field and corresponding stochastic parameters to model their associated uncertainties in magnitude and orientation.

In the following, we assume a discrete sampling of a 2D domain on a Cartesian grid structure¹ with grid points $\mathbb{S}_{m,n} = \{\mathbf{x}_{i,j} : 1 \leq i \leq m, 1 \leq j \leq n\}$. The data uncertainty at every point is modeled by a multivariate random variable \mathbf{Y} with scalar-valued components $Y(\mathbf{x}_{i,j})$. We further assume that the random variables follow a *multivariate Gaussian distribution*, so that the distribution at point $\mathbf{x}_{i,j}$ is characterized by a mean value $\mu(\mathbf{x}_{i,j})$ and a standard deviation $\sigma(\mathbf{x}_{i,j})$. Moreover, the correlation values between any pair of random variables, $\rho(Y(\mathbf{x}_{i,j}), Y(\mathbf{x}_{k,l}))$, can be computed.

3.1 Uncertainty Parameters

In a Gaussian distributed random field, gradients also have an associated probability distribution. We derive these distributions by first approximating the gradients from the given random variables via a linear operator, and then using this operator to approximate the uncertainty parameters, i.e., the means and covariance matrices, from the uncertainty parameters of the random variables.

The gradient at a point $\mathbf{x}_{i,j}$ can be approximated via central differences (one-sided differences at the domain boundaries) on the random variables as

$$\nabla Y(\mathbf{x}_{i,j}) = \mathbf{A}\mathbf{s}(\mathbf{x}_{i,j}). \quad (1)$$

1. In the Appendix we describe the extension to arbitrary grid structures.

Here, the 4-element stencil \mathbf{s} contains the random variables $\mathbf{s}(\mathbf{x}_{i,j}) = [Y(\mathbf{x}_{i+1,j}), Y(\mathbf{x}_{i-1,j}), Y(\mathbf{x}_{i,j+1}), Y(\mathbf{x}_{i,j-1})]^\top$, and the 2×4 matrix \mathbf{A} contains the inverse point distances

$$\begin{aligned} \mathbf{A}_{1,1} &= \|\mathbf{x}_{i+1,j} - \mathbf{x}_{i-1,j}\|^{-1}, \mathbf{A}_{1,2} = -\mathbf{A}_{1,1}, \\ \mathbf{A}_{1,3} &= \mathbf{A}_{1,4} = \mathbf{A}_{2,1} = \mathbf{A}_{2,2} = 0, \\ \mathbf{A}_{2,3} &= \|\mathbf{x}_{i,j+1} - \mathbf{x}_{i,j-1}\|^{-1}, \mathbf{A}_{2,4} = -\mathbf{A}_{2,3}. \end{aligned}$$

Since the stencil $\mathbf{s}(\mathbf{x}_{i,j})$ forms a 4-component subset of the multivariate random variable \mathbf{Y} , its probability distribution is multivariate Gaussian as well. Furthermore, due to the linear relation between ∇Y and \mathbf{s} , the gradient follows a *bivariate Gaussian distribution*. In order to fully describe this distribution, we first need to compute the mean gradient μ_∇ and the covariance matrix Σ_∇ of ∇Y . From Equ. (1), these quantities relate to the means and covariances of the random variables via

$$\mu_\nabla(\mathbf{x}_{i,j}) = \mathbf{A}\mu_s(\mathbf{x}_{i,j}), \quad (2)$$

$$\Sigma_\nabla = \mathbf{A}\Sigma_s\mathbf{A}^\top, \quad (3)$$

where the k -th component of $\mu_s(\mathbf{x}_{i,j})$ contains the mean of the k -th component of $\mathbf{s}(\mathbf{x}_{i,j})$, i.e., $(\mu_s(\mathbf{x}_{i,j}))_k = \mu(\mathbf{s}(\mathbf{x}_{i,j})_k)$, and the components of the covariance matrix Σ_s of the random stencil vector are $(\Sigma_{\mathbf{s}(\mathbf{x}_{i,j})})_{m,n} = \sigma(\mathbf{s}(\mathbf{x}_{i,j})_m)\sigma(\mathbf{s}(\mathbf{x}_{i,j})_n)\rho(\mathbf{s}(\mathbf{x}_{i,j})_m, \mathbf{s}(\mathbf{x}_{i,j})_n)$.

From the given mean gradient and covariance matrix, the bivariate probability distribution function of ∇Y for a vector \mathbf{g} is then derived as

$$p_\nabla(\mathbf{g}) = \frac{1}{2\pi\sqrt{\det\Sigma_\nabla}} \exp(-0.5(\mathbf{g} - \mu_\nabla)^\top \Sigma_\nabla^{-1}(\mathbf{g} - \mu_\nabla)). \quad (4)$$

Since p_∇ describes the likelihood that the gradient takes on a given magnitude or direction, it expresses the uncertainty of the gradient in both strength and orientation. In the following subsections, we separate these two properties, and derive analytic expressions of the distributions for each of them. These distributions are then used to visualize the gradient uncertainty.

3.2 Uncertainty in Derivative

Because the derivative at a spatial point $\mathbf{x}_{i,j}$ in a 2D scalar field is dependent on direction, we first have to select a suitable direction into which to estimate the uncertainty of the derivative. We therefore choose the direction at the respective point into which the derivative is most likely maximum, namely the mean gradient direction in a Gaussian distributed data set.

The uncertainty of the derivative in the mean gradient direction can itself be modeled by a scalar random variable, where the values in the range of this variable are obtained by projecting the gradient random variable onto the mean gradient direction

$$D(\mathbf{x}_{i,j}) := \frac{\mu_\nabla(\mathbf{x}_{i,j})^\top \nabla Y(\mathbf{x}_{i,j})}{\|\mu_\nabla(\mathbf{x}_{i,j})\|}. \quad (5)$$

For the fixed mean gradient direction, $D(\mathbf{x}_{i,j})$ describes the random variation of the derivative along this direction. Because ∇Y is bivariate Gaussian distributed and D is obtained by applying a linear operator to it, D also obeys a Gaussian distribution, with the mean and standard deviation given by

$$\mu_D(\mathbf{x}_{i,j}) = \|\mu_\nabla(\mathbf{x}_{i,j})\|, \quad (6)$$

$$\sigma_D(\mathbf{x}_{i,j}) = \frac{\sqrt{\mu_\nabla(\mathbf{x}_{i,j})^\top \Sigma_\nabla \mu_\nabla(\mathbf{x}_{i,j})}}{\|\mu_\nabla(\mathbf{x}_{i,j})\|}. \quad (7)$$

Thus, the mean derivative in the mean gradient direction is the magnitude of the mean gradient. The standard deviation indicates

the variability of the derivative and serves as an uncertainty indicator. We will subsequently call this uncertainty the derivative uncertainty.

3.3 Uncertainty in Orientation

To study the variability of the gradient direction and, thus, to derive further insight into the stability of geometric features in the data, we now quantify the uncertainty in direction. Therefore, we make use of Equ. (4), which represents the uncertainty in direction, as well as magnitude. In order to isolate the uncertainty in direction, we first perform a coordinate transformation from Cartesian to polar coordinates, and then integrate over the radius coordinate to eliminate the gradient magnitude.

In polar coordinates, the distribution function becomes

$$p_{\nabla}(\theta, r) = \frac{r}{2\pi\sqrt{\det\Sigma_{\nabla}}} \exp(E(\theta)), \quad \theta \in [0, 2\pi], \quad r \in [0, \infty[\quad (8)$$

$$E(\theta) = \left(-\frac{1}{2} \left(r \begin{pmatrix} \cos\theta \\ \sin\theta \end{pmatrix} - \mu_{\nabla} \right)^{\top} \Sigma_{\nabla}^{-1} \left(r \begin{pmatrix} \cos\theta \\ \sin\theta \end{pmatrix} - \mu_{\nabla} \right) \right).$$

For every angle θ , a probability density value can be obtained by integrating the bivariate gradient distribution along a line from radius $r = 0$ to $r = \infty$, i.e., by evaluating the θ -marginal

$$p_{\nabla}^{\theta}(\theta) = \int_0^{\infty} p_{\nabla}(\theta, r) dr, \quad \theta \in [0, 2\pi]. \quad (9)$$

The line of integration in the 2D density function is illustrated in Fig. 4 (a). The closed form solution of this integral is²

$$p_{\nabla}^{\theta}(\theta) = \frac{\exp(-H(\mu_{\nabla_x}, \mu_{\nabla_y})) (1 - \sqrt{\pi} t \exp(t^2) (1 - \operatorname{erf}(t)))}{4\pi\sqrt{\det\Sigma_{\nabla}} H(\cos\theta, \sin\theta)}, \quad (10)$$

with the auxiliary terms

$$H(x, y) = \frac{1}{2(1 - \rho_{\nabla}^2)} \left(\frac{x^2}{\sigma_{\nabla_x}^2} + \frac{y^2}{\sigma_{\nabla_y}^2} - 2\rho_{\nabla} \frac{xy}{\sigma_{\nabla_x}\sigma_{\nabla_y}} \right), \quad (11)$$

$$t = \frac{-\mu_{\nabla_x}\sigma_{\nabla_y}^2 \cos\theta - \mu_{\nabla_y}\sigma_{\nabla_x}^2 \sin\theta}{2\det\Sigma_{\nabla}\sqrt{H(\cos\theta, \sin\theta)}} + \frac{\rho_{\nabla}\sigma_{\nabla_x}\sigma_{\nabla_y}(\mu_{\nabla_x}\sin\theta + \mu_{\nabla_y}\cos\theta)}{2\det\Sigma_{\nabla}\sqrt{H(\cos\theta, \sin\theta)}}. \quad (12)$$

Here, μ_{∇_x} and μ_{∇_y} are the components of the mean gradient vector μ_{∇} , while σ_{∇_x} and σ_{∇_y} are the standard deviations of the gradient components (square roots of the diagonal entries of Σ_{∇}), and $\rho_{\nabla} = \Sigma_{\nabla_{xy}}/(\sigma_{\nabla_x}\sigma_{\nabla_y})$ is the corresponding correlation value. These values can be computed at every grid point (cf. Equ. (2) and (3)).

In 3D, the uncertainty in the gradient orientation is obtained similarly to the 2D case, by performing a change of variables from the Cartesian coordinates, x , y , and z , to the spherical coordinates, radius r , polar angle θ , and azimuthal angle ϕ , and integrating over the radius to isolate the gradient orientation from the magnitude. The derivation, available online at [3], is done by first writing the θ, ϕ -marginal like the product of a second-order polynomial and a Gaussian function, and then integrating the resulting function over the radius from $r = 0$ to $r = \infty$. Unlike in the 2D case (cf. Appendix), the polynomial is no longer linear, but quadratic, due the Jacobian of the coordinate transformation.

Equ. (10) expresses the probability distribution of the gradient direction. As we are interested in using the probability distribution for assessing the stability of the orientation of certain geometric

structures in the data (e.g., the orientation of an iso-contour at a certain location), the probability of occurrence of angle θ should include the probability of occurrence of $\theta + \pi$. To account for this, we introduce the function

$$p_{\leftrightarrow}(\theta) = p_{\nabla}^{\theta}(\theta) + p_{\nabla}^{\theta}(\theta + \pi), \quad \theta \in [0, \pi], \quad (13)$$

which adds the two probability distributions of the positive and negative gradient direction, and, thus, expresses the probability distribution of the undirected orientation uncertainty.

To obtain a single parameter indicating the degree of orientation uncertainty, we have built upon the concept of *circular variance* (cf. [34]) to introduce the following scalar measure for the orientation uncertainty

$$\zeta = 1 - \left\| \int_0^{\pi} p_{\leftrightarrow}(\theta) \begin{pmatrix} \cos 2\theta \\ \sin 2\theta \end{pmatrix} d\theta \right\| \in [0, 1]. \quad (14)$$

For a low orientation uncertainty of the gradient, the unit vectors $(\cos 2\theta, \sin 2\theta)^{\top}$ pointing into the likely direction are weighted by high values of p_{\leftrightarrow} and ζ approaches zero. On the contrary, for a high orientation uncertainty, the distribution p_{\leftrightarrow} tends to become uniform and all vectors obtain the same weight. In this case, the circular variance approaches one. Thus, the circular variance acts as a normalized indicator of the spread in gradient orientation.

4 VISUALIZATION

The gradient uncertainty at a certain point in the domain comprises the derivative uncertainty and the uncertainty in the gradient orientation. So far, we have derived the probability distributions describing the spread in both quantities. In the following, we propose separate visualization techniques for these distributions.

4.1 Uncertainty in Derivative

Our goal is to provide a visualization that shows simultaneously the shape of iso-contours in the initial mean values, the distribution of the mean gradient magnitudes (μ_D), and the derivative uncertainty at every point in the domain. In particular, we are interested in a visualization that allows classifying points according to their respective *lower confidence boundaries* $\mu_D - \sigma_D$. The rationale is that a gradient is likely to disappear or even to invert, depending on whether $\mu_D - \sigma_D$ is close to zero or negative, classifying the slope along the gradient direction at this point as rather unstable. Only for a strongly positive $\mu_D - \sigma_D \gg 0$ can this characteristic be regarded as stable. The visualization of iso-contours, on the other hand, gives important contextual information regarding the orientation of gradients in the mean values.

4.1.1 Derivative Diffusion Mapping

To convey the basic shapes of the iso-contours in the mean scalar field, as well as the spatial differences in the mean derivative, we use patterns that are oriented according to the iso-contours, and vary with a frequency indicating the derivative strength. To this purpose, we start by partitioning the range of mean values into a number of N equally spaced intervals. Each interval has a width of $(\mu_{\max} - \mu_{\min})/N$, where μ_{\min} and μ_{\max} are the smallest and largest mean value, respectively. Each interval is assigned either the black or white color, in alternating order. At a grid point $\mathbf{x}_{i,j}$, the mapping of the data value to color is performed via

$$\kappa(\mathbf{x}_{i,j}) := \left\lfloor \frac{\mu(\mathbf{x}_{i,j})N}{\mu_{\max} - \mu_{\min}} \right\rfloor \bmod 2, \quad (15)$$

2. The derivation of the closed form solution is given in the Appendix.

where $\mu(\mathbf{x}_{i,j})$ is the mean value at this point. An example showing the resulting black and white pattern is given in Fig. 1 (a). In regions where the derivative in mean gradient direction is low, the white and black bands are stretched, narrowing with increasing derivative. The principal shape of the iso-contours reflects in the shape of the bands.

To visually encode the confidence intervals $[\mu_D - \sigma_D, \mu_D + \sigma_D]$ into the contour map, we introduce a *diffusion* process that smears out the sharp transitions between the black and the white bands. Over time, the colors diffuse, so that, in the limit, the bands turn into gray and no contrast can be seen anymore. We show later how to use the diffusion time as a parameter to locally control the amount of diffusion depending on the confidence intervals.

The simulated diffusion process is anisotropic, meaning that the diffusion takes place along a particular direction (and its inverse direction) through the bands and, possibly, through the boundaries between two neighboring bands. The diffusion at a certain point occurs along the *normal curve*, which is the curve passing through the point and oriented along the gradient direction. Thus, a normal curve crosses the boundary between two bands orthogonally (see the blue curve in Fig. 1 (a)).

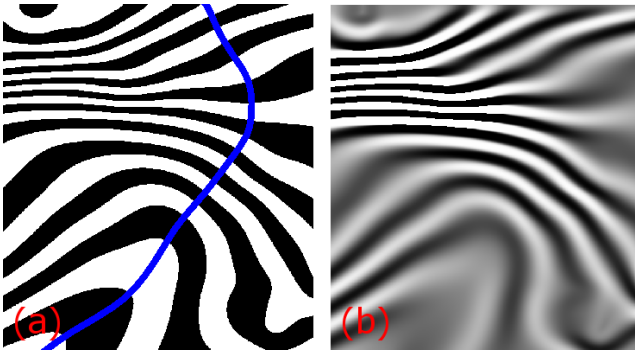


Fig. 1. (a) A 2D scalar field is shown. The data range is partitioned into equally spaced intervals, colored black and white. The thickness of the resulting bands reveals the local gradient magnitude. The blue normal curve is everywhere tangential to the gradient field. (b) The gradient magnitude is also encoded as color diffusion (high and low diffusion in regions with low and high gradient magnitudes).

Because of the diffusion, the color at a certain point can change over time, from only black or white (no diffusion), to a mixture of 50% black and 50% white (full diffusion). The fraction of the initial black or white color, respectively, is called *diffusion value*. By varying the diffusion time, we can control the *degree of diffusion*. Note that the fraction of the initial color (diffusion value) is 1, if no diffusion takes place (low degree of diffusion), and approaches 0.5 for higher diffusion degrees. Low and high degrees of diffusion are associated with high and low diffusion values. Furthermore, only in the limit are the diffusion values homogenous along the normal curve within one band. For small degrees of diffusion (low diffusion time), the diffusion values are lower close to the band boundaries.

Instead of simulating a physical diffusion process at run-time, we pre-compute a 2D diffusion texture, and look up the actual diffusion value at a certain spatial point and for a certain diffusion degree from this texture. The 2D texture contains diffusion values between 1 (no diffusion) and 0.5 (full diffusion). These values model the fraction of the initial color in the final color mix after the diffusion time has passed. The texture T is parameterized over the relative position u of a point between the two boundary lines

of the band containing this point (from 0 to 1), and the degree of diffusion v (from 0 to 1).

T is obtained in two steps. First, an intermediate 2D texture τ is created, parameterized over the diffusion time v_τ from 0 to a selected maximum $v_{\tau_{\max}}$, and over the relative point position ($u_\tau = u$). The values of τ at the texture coordinates (u_τ, v_τ) are computed by a convolution of the *periodic box function*

$$\beta(x) := [x] \bmod 2, \quad x \in \mathbb{R} \quad (16)$$

with a Gaussian kernel G_{v_τ} with standard deviation v_τ :

$$\begin{aligned} \tau(u_\tau, v_\tau) &= (G_{v_\tau} * \beta)(u_\tau) \\ &= \frac{1}{v_\tau \sqrt{2\pi}} \int_{-\infty}^{\infty} \exp\left(-\frac{(x-u_\tau)^2}{2v_\tau^2}\right) \beta(x) dx. \end{aligned} \quad (17)$$

Here, β describes the periodic black and white pattern along the normal curve in the data domain, independent of the concrete frequency of the black and white pattern along this curve in the spatial domain.

The greater v_τ is in Equ. 17, the larger the extent of the filter kernel and the more β is smoothed, simulating an increasing diffusion time. For a constant v_τ , the closer the points are to the boundaries between two bands, the more values from the respective other band will be integrated, introducing lower diffusion values at the boundaries.

The next step performs a parameter transformation, so that the v texture coordinates are $\in [0, 1]$ instead of $\in [0, v_{\tau_{\max}}]$. This is achieved via the mapping

$$\lambda(v_\tau) = 2 \int_0^1 \tau(u_\tau, v_\tau) du_\tau - 1, \quad (18)$$

which is strictly monotonic from 1 to 0 for $v_\tau \in [0, v_{\tau_{\max}}]$. Because we need to map from $v \in [0, 1]$ to $v_\tau \in [0, v_{\tau_{\max}}]$, the inverse function λ^{-1} is needed. While this does not have a closed form, it can be obtained using a back-mapping strategy between the domain $[0, v_{\tau_{\max}}]$ and its image $\lambda([0, v_{\tau_{\max}}])$. The values in the diffusion texture T , shown in Fig. 2 for $u \in [0, 1]$ and $v \in [0, 1]$, are finally computed as

$$T(u, v) = \tau(u, \lambda^{-1}(v)), \quad u \in [0, 1], \quad v \in [0, 1]. \quad (19)$$

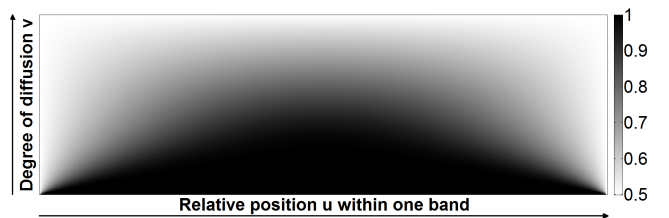


Fig. 2. The diffusion texture T . Diffusion values from 0.5 to 1 are mapped to a grayscale color map. The x-axis represents the relative position u of a point between two band boundaries. The y-axis represents the degree of diffusion v .

As stated before, the parameter v should control the degree of diffusion depending on the strength of the derivative in the mean gradient direction. Thus, we finally make v dependent on the random variable D (cf. Equ. 6), which models the derivative in the mean gradient direction. For a point $\mathbf{x}_{i,j}$, the texture coordinates

are now computed as

$$u(\mathbf{x}_{i,j}) = \frac{\mu(\mathbf{x}_{i,j})N}{\mu_{\max} - \mu_{\min}} - \left\lfloor \frac{\mu(\mathbf{x}_{i,j})N}{\mu_{\max} - \mu_{\min}} \right\rfloor, \quad (20)$$

$$v(\mathbf{x}_{i,j}) = \max \left(\min \left(\frac{D(\mathbf{x}_{i,j})}{\max_{\mathbf{x} \in \mathbb{S}_{m,n}} \mu_D(\mathbf{x})}, 1 \right), 0 \right). \quad (21)$$

The u -component determines the position within one band between the band boundaries, and the v -component maps D to the degree of diffusion. Because it uses the relative position between the maximum mean derivative in mean gradient direction and zero, high and low diffusion degrees are assigned to low and high derivative values, respectively.

One diffusion value $T(u, v)$ is obtained for each point $\mathbf{x}_{i,j}$ in the data field. To smear out the black and white bands, the value $1 - T(u, v)$ is either subtracted from (white) or added to (black) the intensity value. Thus, in regions with a low derivative D , the bands turn into gray, whereas in regions with strong derivatives, the black and white bands remain well separated.

This process is simulated by introducing *normalized diffusion values*

$$\tilde{T}(u, v) := 2T(u, v) - 1 \in [0, 1], \quad (22)$$

and computing the final color $c(\mathbf{x}_{i,j})$ at each grid point by blending an RGB *diffusing color* c_d over a *background color* c_b :

$$c(\mathbf{x}_{i,j}) = (1 - \tilde{T}(u, v))c_d(\mathbf{x}_{i,j}) + \tilde{T}(u, v)c_b(\mathbf{x}_{i,j}). \quad (23)$$

Fig. 1 (b) shows an example where the variable D in Equ. (21) was replaced by the mean derivative μ_D . The background color is either black or white, depending on which band $\mathbf{x}_{i,j}$ belongs to, and the diffusing color is gray ($c_d = (0.5, 0.5, 0.5)$). Even though this visualization does not reveal any new information, because μ_D is now encoded twice, once as stripe pattern and once as diffusion, it illustrates the use of diffusion as an additional means for data classification. We will later show how to select the diffusion colors (and diffusion values) locally at each point depending on the mean gradient magnitude and the confidence interval. In this way we can simultaneously encode the three characteristic confidence values $\mu_D - \sigma_D$, μ_D , and $\mu_D + \sigma_D$ in one single view.

4.1.2 Diffusion Coloring

To encode the uncertainty of the derivative in mean gradient direction (cf. 3.2), we use the proposed diffusion scheme in combination with a set of three different diffusion colors. The goal is to use the degree of color diffusion over the black and white bands for classifying regions with respect to the following four categories: a) strong mean derivative and low uncertainty, b) strong mean derivative and high uncertainty, c) low mean derivative and low uncertainty, and d) low mean derivative and high uncertainty.

To encode the confidence interval of the derivative into diffusion, the variable D in Equ. (21) is replaced by the three characteristic confidence values $\mu_D - \sigma_D$, μ_D , and $\mu_D + \sigma_D$. Thus, one obtains the normalized diffusion values

$$\tilde{T}_D^-(\mathbf{x}_{i,j}) = \tilde{T} \left(u(\mathbf{x}_{i,j}), \max \left(\frac{\mu_D(\mathbf{x}_{i,j}) - \sigma_D(\mathbf{x}_{i,j})}{\max_{\mathbf{x} \in \mathbb{S}_{m,n}} \mu_D(\mathbf{x})}, 0 \right) \right), \quad (24)$$

$$\tilde{T}_D^0(\mathbf{x}_{i,j}) = \tilde{T} \left(u(\mathbf{x}_{i,j}), \frac{\mu_D(\mathbf{x}_{i,j})}{\max_{\mathbf{x} \in \mathbb{S}_{m,n}} \mu_D(\mathbf{x})} \right), \quad (25)$$

$$\tilde{T}_D^+(\mathbf{x}_{i,j}) = \tilde{T} \left(u(\mathbf{x}_{i,j}), \min \left(\frac{\mu_D(\mathbf{x}_{i,j}) + \sigma_D(\mathbf{x}_{i,j})}{\max_{\mathbf{x} \in \mathbb{S}_{m,n}} \mu_D(\mathbf{x})}, 1 \right) \right). \quad (26)$$

These values are encoded into the visualization via three different color mappings, and a special blending and interpolation scheme.

We use the blending equation (23) to assign a specific color to each grid point. Because we are interested in identifying regions where the lower confidence boundary $\mu_D - \sigma_D$ is significantly positive — indicating a stable positive derivative in the mean gradient direction — the diffusion value in Equ. (23) is replaced by $\tilde{T}_D^-(\mathbf{x}_{i,j})$. Thus, the final color induced by the lower confidence boundary derivative is

$$c(\mathbf{x}_{i,j}) = (1 - \tilde{T}_D^-(\mathbf{x}_{i,j}))c_d(\mathbf{x}_{i,j}) + \tilde{T}_D^-(\mathbf{x}_{i,j})c_b(\mathbf{x}_{i,j}), \quad (27)$$

where c_d is a selected diffusion color. In regions where the lower confidence boundary derivative has a low value (e.g., close to zero), c_d diffuses over the black and white bands. On the other hand, in regions with a significantly positive lower boundary, the diffusion is low as well, and the black and white bands are not affected.

The diffusing color c_d encodes the relative position of the values $\mu_D - \sigma_D$, μ_D , and $\mu_D + \sigma_D$ with respect to the zero derivative. Therefore, the color maps $CM_b = [\text{cyan} \rightarrow \text{blue} \rightarrow \text{magenta}]$ and $CM_w = [\text{yellow} \rightarrow \text{red} \rightarrow \text{magenta}]$ are defined for the black and white band, respectively. The RGB colors $CM_b(i)$ and $CM_w(i)$ are obtained from each map using an index $i \in [0, 1]$, where $i = 1$ corresponds to magenta.

The colors are used to indicate the characteristics of the confidence intervals in three levels: Cyan and yellow correspond to the lower confidence boundary (level 1), blue and red to the mean derivative (level 2), and magenta to the upper boundary (level 3). At first, the position of the mean derivative is encoded. If μ_D is significantly positive, only the level-1 color is used, while for a low μ_D value, the level-2 color dominates. The index $i_{1/2}$ used to retrieve the color interpolated between the level-1 and level-2 colors is computed from the diffusion value of the mean derivative as follows

$$i_{1/2} = 0.5(1 - \tilde{T}_D^0(\mathbf{x}_{i,j})). \quad (28)$$

The level-3 color encodes the position of the upper confidence boundary $\mu_D + \sigma_D$. If it is strongly positive, the color does not change. If, on the other hand, $\mu_D + \sigma_D$ also approaches zero, the color is shifted towards magenta via the diffusion value of the upper boundary. Thus, the final index to map into the diffusion color is

$$i = \tilde{T}_D^+(\mathbf{x}_{i,j})i_{1/2} + (1 - \tilde{T}_D^+(\mathbf{x}_{i,j})). \quad (29)$$

The diffusing color c_d is then set to either $CM_b(i)$ or $CM_w(i)$, depending on the background color, and the final color is obtained by using the diffusing color in the blending equation (27). Note that using the diffusion values associated to the respective confidence values, instead of using these values directly for the color coding, generates a smooth visualization of the derivative confidence intervals.

Fig. 3 shows four examples demonstrating the proposed color mapping using different mean derivatives and derivative uncertainties. On the left, the mean derivative values (blue) are plotted on a linear 1D scale, the zero derivative being marked by the black circle. Furthermore, the confidence regions between the upper and lower boundaries are visualized as red bands, and the two boundary derivatives as red dots.

On the right hand side, we show the cross section along a normal curve through two neighboring black and white bands. In (a), the mean derivative in mean gradient direction is significantly positive, while the standard deviation is relatively low. Therefore, the black and white color is not covered by the level-1 colors, as

the lower confidence boundary is significantly greater than zero. In (b), the mean value is the same as in (a), but the standard deviation is higher. This results in the coverage of the black and white stripes by the level-1 colors (cyan and yellow). In (c), the mean value is close to zero. Thus, the level-2 colors dominate. The black and white pattern is completely covered, because the lower confidence boundary is also close to zero. The strong diffusion of the level-3 color (magenta) indicates that the upper confidence boundary is also close to zero and, thus, the uncertainty is low. In (d), the uncertainty is larger than in (c), resulting in a significantly increased upper confidence boundary and a lower diffusion of the level-3 color. This reveals a low mean derivative, yet, due to the high uncertainty, stronger positive and negative derivatives are likely to occur. For further illustration of the specific color coding we propose, including different settings for μ_D and σ_D , we refer the reader to the video accompanying this manuscript.

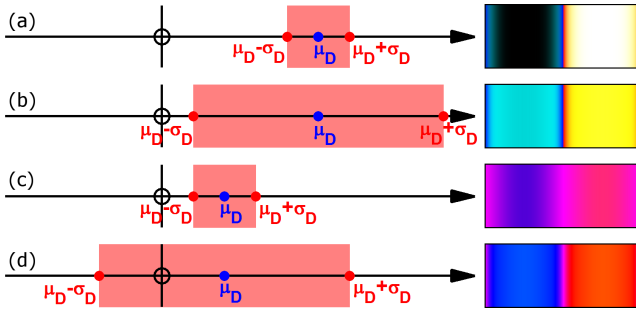


Fig. 3. Color maps for diffusion coloring of confidence intervals. Four different maps are used to classify different combinations of μ_D and σ_D . On the right, for each of the intervals, the respective coloring and diffusion along a normal curve through two adjacent black and white bands are illustrated.

4.2 Uncertainty in Orientation

To visualize the uncertainty in orientation, the orientation probability density and the circular variance (cf. Equ. (13) and (14)) are encoded into a circular glyph representation. Each glyph is represented by a triangle fan, comprising a number of equally sized triangles that are arranged around the glyph center-point (see Fig. 4). For each triangle, color and transparency values are assigned to the two off-center vertices, while the center vertex is assigned the mean color and transparency of these vertices. Starting with $\theta_0 = 0$ at the east vertex, each off-center vertex i is assigned an angle $\theta_i = 2\pi(i/N)$ in counterclockwise order, where N is the number of off-center vertices. This ordering is illustrated in Fig. 4 (b). An orientation probability density value is computed at every off-center vertex by evaluating Equ. (13) at the assigned θ_i for $\theta_i \leq \pi$ and at $\theta_i - \pi$ for $\theta_i > \pi$. The gradient uncertainty parameters μ_{∇} and Σ_{∇} , which are assumed to be constant for the entire glyph, are computed at the data point at which the glyph is centered.

All vertices of a glyph have the same color, which encodes the degree of uncertainty. The color of a glyph is obtained by mapping the circular variance ζ at the glyph center point to color via a predefined color map. In our example, we use the mapping $[0, 1] \rightarrow [\text{green} \rightarrow \text{cyan} \rightarrow \text{blue} \rightarrow \text{magenta} \rightarrow \text{red}]$. Thus, glyphs in regions with very low and very high gradient orientation uncertainty tend to green and red, respectively. To allow the user to distinguish between points at which the orientation distribution is more or less uniform, i.e., to show the individual distributions per glyph,

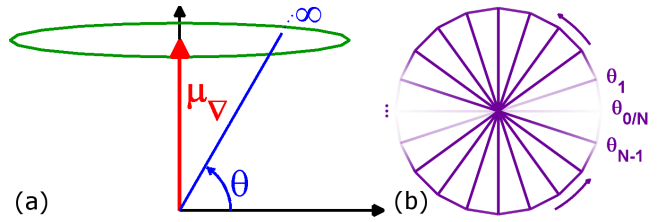


Fig. 4. (a) 2D Gaussian probability density of a vector quantity. The red arrow and green ellipse indicate the mean direction and confidence region, respectively. The gradient direction probability $p_{\nabla}^{\theta}(\theta)$ for an angle θ is obtained by integrating the 2D probability density function along the blue line from 0 to ∞ . (b) Triangle-based glyph representation. Each off-center vertex at angle θ_i is assigned a transparency according to the probability density function p_{\leftrightarrow} of the angular orientation. The color is constant for all vertices and determined by the circular variance of p_{\leftrightarrow} .

the transparency of the glyphs is modified accordingly. By setting the transparency of a vertex to

$$\alpha(\theta) = \frac{p_{\leftrightarrow}(\theta)}{\max_{\theta \in [0, \pi]} p_{\leftrightarrow}(\theta)}, \quad (30)$$

glyphs representing a uniform distribution become fully opaque. On the other hand, varying transparencies causes a clear color contrast between orientations with high and low likelihoods.

Fig. 6 shows four examples of bivariate gradient distributions and the corresponding uncertainty glyphs. The mean gradient μ_{∇} is shown as a red vector, the green ellipse, related to Σ_{∇} , indicates the 2D confidence area around the mean vector, and the black line represents the mean orientation of the vector. The glyphs are colored according to the color map for the circular variance.

In (a), the orientation uncertainty is low, because the gradient variation mainly alters the magnitude. In (b), there is a significant uncertainty in orientation. The transparency mapping further indicates a multi-modal orientation distribution, i.e., two significant different orientations are equally likely. Note that the orientation of the mean vector has a low likelihood and is, therefore, unstable. In (c), the zero correlation between the gradient's components in (a) and (b) was changed to a negative value. This resulted in an asymmetric orientation distribution with respect to the mean vector. In (d), the mean gradient is the zero vector. Although the glyph indicates a strong uncertainty, it becomes apparent that the gradient is most likely directed vertically.

Because the user is interested in the orientation stability of the gradients, the mean data set is displayed as a contour representation. A user-specified number of iso-lines is displayed for iso-values equidistantly positioned within the data range.

A glyph-based visualization, such as the one in Fig. 8 (b), facilitates a rapid understanding of the way uncertainty affects the orientation of the gradients, especially in the regions with lower uncertainty, where the glyphs become less opaque and the geometry of the iso-contours can be visualized concurrently with its uncertainty. This happens irrespective of the placement of the glyphs, because the pattern of the glyphs is typically orthogonal to the iso-contours of the scalar field, making the contours clearly discernible. An alternative would be to consider the orientation uncertainty of the tangent line, rather than that of the gradient, but this would not only produce no new information, it would also lower the contrast in coverage of the iso-contours between low and high uncertainty regions.

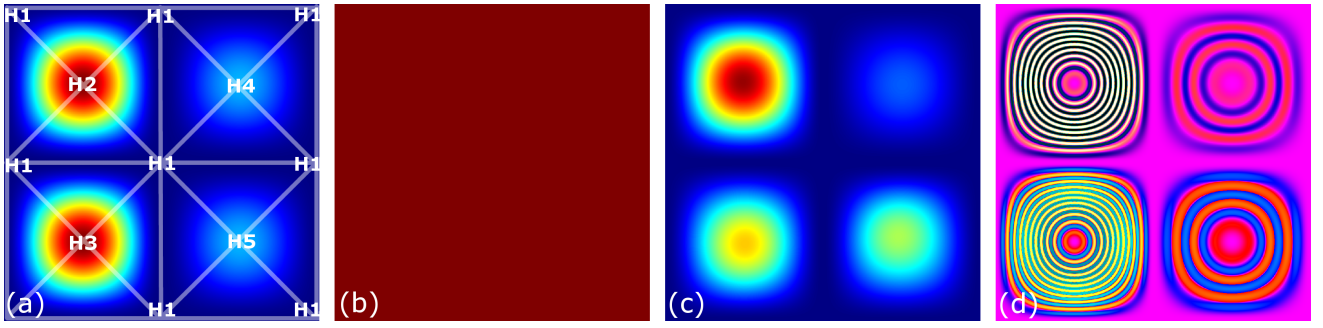


Fig. 5. (a) Mean values in a synthetic 2D ensemble data set. Data values at vertices of a triangular grid are generated via Gaussian distributed random variables H_i , data interpolation is used in between. (b) The standard deviation of each variable is constant over the entire domain, but different correlations were enforced between the variables H_i . (c) One particular ensemble member (realization) is shown. Even though every random variable has the same standard deviation, one can observe vastly different data distributions, and gradient variations thereof. (d) Visualization of derivative uncertainty via color diffusion. Upper left cell: Strong mean derivative and low derivative uncertainty is indicated by black and white striping. Lower left cell: Diffusing cyan and yellow indicates strong mean derivative and high derivative uncertainty. Upper right cell: Diffusing magenta over red and blue color indicates low mean derivative and low derivative uncertainty. Lower right cell: Vanishing magenta indicates low mean derivative and strong derivative uncertainty.

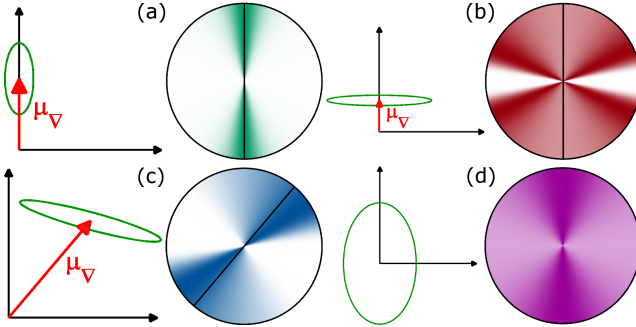


Fig. 6. 2D gradient distributions and corresponding circular glyphs. A black line encodes the mean gradient orientation. (a) High gradient magnitude and low orientation uncertainty. (b) Multi-modal probability distribution. Two orientations are equally likely, the mean orientation is very unlikely and therefore unstable. (c) Asymmetric spread of the orientation. (d) Zero mean gradient, but strong likelihood of a vertical gradient orientation.

5 RESULTS AND DISCUSSION

To evaluate our techniques, we first use a synthetic 2D scalar field, which was designed to specifically demonstrate the kind of insights these techniques provide (see Fig. 5). The 2D domain is divided into 2×2 quadratic cells. Scalar values are given at grid points of a triangular grid (cf. transparent grid lines in (a)). The values at the cell corners and cell centers (grid points) are modeled via a multivariate Gaussian random variable \mathbf{H} . The first component, H_1 , models the values at all corners of the four cells, its mean being set to $\mu(H_1) = 0$. The values at the centers of the upper and lower cells, respectively, are modeled via four components H_2, H_3, H_4 , and H_5 , with means $\mu(H_2) = 1$, $\mu(H_3) = 1$, $\mu(H_4) = 0.3$, and $\mu(H_5) = 0.3$. Inside each cell and triangle, C^1 -interpolation between the values at the corner points and the center point is performed. In (a), the mean data values are shown.

The standard deviation of all random variables is set to the constant value $\sigma(H_i) = 1$, as shown in (b). A strongly positive correlation is modeled between the random variables H_1 and H_2 ,

and between H_1 and H_4 . All other pairs are uncorrelated (pairwise correlation equals zero). An ensemble of realizations for \mathbf{H} can now be generated at the corner and center points via a multivariate Gaussian random generator. One realization (ensemble member) for \mathbf{H} and its interpolation is shown in (c).

In (d), the technique proposed in subsection 4.1 was used to visualize the derivative uncertainty. In the upper left cell, the mean gradient magnitude is high. As H_1 and H_2 are strongly correlated³, i.e., the random values go up and down simultaneously, the derivative is stable. This stability is indicated by our approach, as the black and white stripes are not covered by the level-1 colors. The corresponding confidence interval relates to the one in Fig. 3 (a). Then, because H_1 and H_3 are uncorrelated, the strong derivative in the lower left cell is not stable. Thus, the bands are completely covered by the level-1 colors. The corresponding confidence interval relates to the one in Fig. 3 (b). Furthermore, the low mean derivative in the upper right cell is conveyed by a strong diffusion of the level-2 colors. As there is also a significant diffusion of the level-3 color magenta, the upper confidence boundary is close to the mean derivative and, therefore, the derivative uncertainty is low (cf. configuration (c) in Fig. 3). The zero correlation between H_1 and H_5 causes a high derivative uncertainty in the lower right cell. This results in a low diffusion of the level-3 color, as shown in Fig. 3 (d).

The example illustrates that our diffusion technique can be used to analyze the stability of certain features in the data with respect to their derivative strength. Comparing the left two cells, only the strong increase of the mean data values towards the center point is stable in the upper left cell. On the other hand, in the lower left cell, the increase could be, due to uncertainty, considerably lower or even negative. Notably, this information cannot be revealed by visualizing only the standard deviation, as shown in Fig. 5 (b). Because it is constant over the whole 2D domain, the standard deviation does not provide any information on the different gradient uncertainties of the data in the cells. Obviously, the diffusion mapping in (d) can provide additional information on the derivative stability, which cannot be revealed by the mean (a) and standard deviation (b), that are usually used

3. A detailed interpretation of correlation in the context of relative uncertainties can be found in [23] and [22].

in uncertainty visualization scenarios.

In the next example, we demonstrate the use of our techniques for analyzing the gradient uncertainty in a geophysics ensemble data set, showing material variations at a certain depth in the earth's crust. The data set was obtained using seismic tomography and contains an ensemble of relative velocity values for shear waves, originating from earthquake source locations. For details on how the data was acquired and the information contained in this data, we refer the reader to [35]. Fig. 7 (a) and (b) show the mean values and the standard deviations at each point in the covered 2D domain. The mean values are mapped linearly from blue (negative) to red (positive). Two important circular features can be observed in the mean values, but the standard deviations in both regions are almost constant. Thus, an uncertainty analysis using only mean values and standard deviations would not reveal any significant differences between the two features.

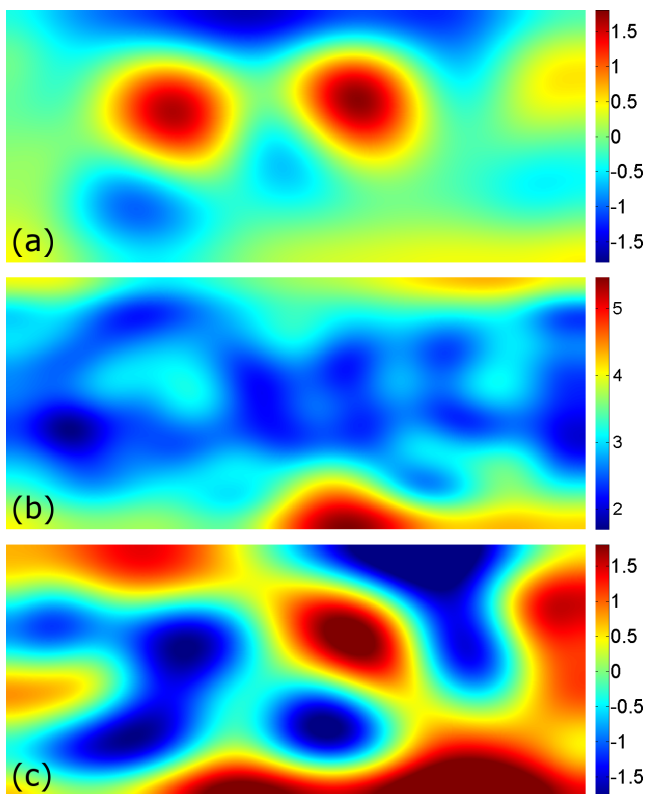


Fig. 7. Mean values (a) and standard deviations (b) in an ensemble of 2D seismic tomography shear wave velocity variations. Two circular features with very similar occurrences can be distinguished. One member (realization) of the ensemble is shown in (c).

In Fig. 8 (a), diffusion coloring was used to visualize the derivative uncertainty. The visualization indicates in the left region a high variation of the derivative in mean gradient direction towards the feature center; the black and white stripes are much more covered by the level-1 colors. This is supported by the visualization of one ensemble member in Fig. 7 (c), which shows strongly positive gradients in the right region, but negative gradients in the left region, i.e., the derivative in the left region is more or less inverted. Diffusion coloring shows this strong derivative uncertainty directly. Fig. 8 (b) illustrates, on the other hand, that the gradient orientation is quite stable in both regions. Thus, both features have a circular structure, yet only for the right

feature can the positive gradient magnitude be assumed stable. In the left circular region it could be possible that the values decrease towards the feature center.

From an application point of view, the visualization helps to identify regions where significant material anomalies are present with respect to the surrounding structures. In the presented example, the data contains relative velocity values for earthquake shear waves. These values are characteristic for certain material structures in the earth's crust. The user is interested to identify local and global maxima and minima of the relative velocity values, because they can serve as indicators for material anomalies (minerals, sediments, ores, oil, etc.) in the earth. Since seismic tomography data sets are always affected by uncertainty, the user is interested in analyzing the respective critical areas (maxima, minima, strong gradients, etc.) with respect to their stability. As demonstrated, the techniques proposed in this work can effectively enable such an analysis.

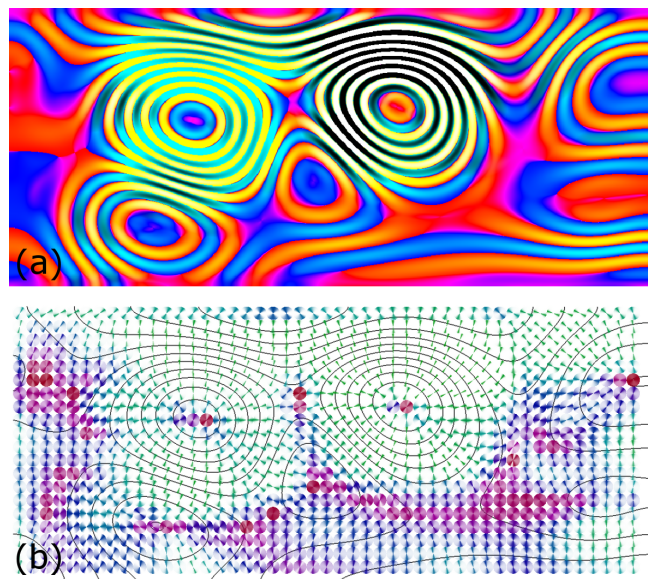


Fig. 8. Visualization of the gradient uncertainty in the ensemble shown in Fig. 7. a) The two circular features can be classified as stable (right feature) and unstable (left feature) with respect to their derivative uncertainty, i.e., strong color diffusion towards level-1 colors cyan and yellow in the left region. b) Glyph-based visualization conveys high stability of the gradient orientation for the left and right features. In contrast, the small circular feature in the bottom left part is significantly affected by orientation uncertainty, indicating a very likely change in the orientation of iso-contours passing through this region.

In our second example, we use uncertainty visualization to identify stable features in the mean values of an ensemble of temperature fields. The ensemble was simulated by the European Center for Medium-Range Weather Forecast (ECMWF) for two different forecast periods and pressure levels above Europe. Mean temperature values, as well as standard deviations and correlations, were computed from the ensemble members.

The mean temperature is shown in Fig. 9 (a). Values are linearly mapped from blue to red (cold-to-warm mapping). In (b), the standard deviation is shown in temperature units, linearly mapped from blue (low) to red (high). Diffusion coloring and glyph-based visualization of the orientation uncertainty are shown in (c) and (d), respectively. The first interesting observation is the high

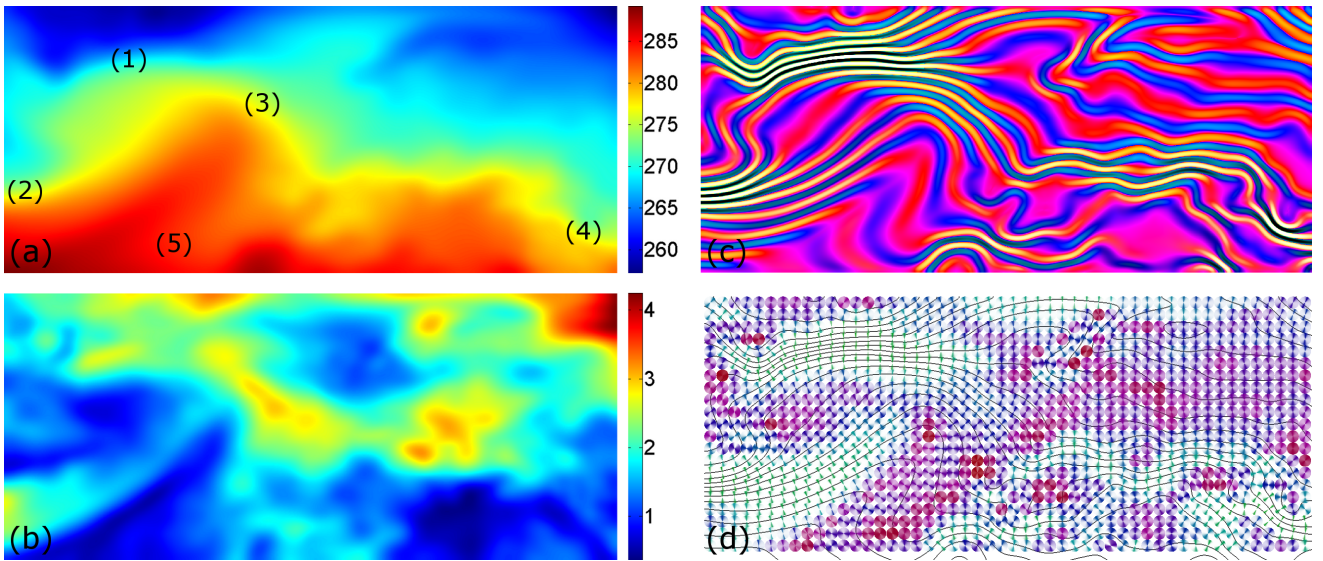


Fig. 9. Mean values (a) and standard deviations (b) of a temperature ensemble forecast. Diffusion coloring is shown in (c). Strong mean gradients with low derivative uncertainty are identified in regions (1), (2) and (4). Color diffusion towards cyan and yellow reveals a strong derivative uncertainty in (3). Strong diffusion towards magenta in (5) indicates a low mean derivative with low uncertainty. The visualization of the uncertainty in gradient orientation (d) reveals stable orientations of iso-contours in (1), (2) and (4).

stability of the strong temperature incline in region (1), which is indicated by the narrow bands and almost no color diffusion on these bands in (c), as well as by the green glyph pattern in (d). Thus, the temperature difference between the blue and cyan region is well resolved, affected by a relatively low uncertainty and significantly different from zero. Interestingly, the standard deviation is relatively strong in this region (cf. (b)). Consequently, the standard deviation does not necessarily allow drawing any conclusion on the variability of derivative strengths, which is also affected by correlation effects. By analyzing in Fig. 9 (c) the transition zone between cyan and red as shown in Fig. 9 (a), one can observe that only the derivatives in (2) and (4) are stable. Although region (3) is affected by a similar mean derivative, the significant diffusion by the level-1 colors indicates with a high probability that the derivative becomes zero. Reliable assumptions on the temperature difference can only be made for the regions of strong derivatives (1), (2) and (4). The strong appearance of the level-3 color in region (5) indicates not only low mean derivatives, but also low uncertainties.

In (d), the uncertainty glyphs, together with the circular variance color mapping, are shown. The orientation of the gradients and therefore the iso-lines are stable in regions (1), (2) and (4). Although in region (3) a similar gradient strength and a clear orientation can be perceived in the mean data (a), the gradient orientation is affected by higher uncertainty and the structure of the transition zone is not well resolved.

The fourth example shows another ECMWF forecast, with the difference that on this occasion it was simulated using a shorter forecast period and a different pressure level. In Fig. 10 (a), the mean data is shown. The uncertainty visualizations in (c) and (d) reveal a very prominent structure in region (1), which is stable with respect to derivative strength and gradient orientation. This stable structure cannot easily be identified using only the mean and the standard deviation. Another interesting region is the transition zone between blue and red in (2), where the standard deviation in (b) shows a significant strong uncertainty. This uncertainty in

the scalar values affects the uncertainty in the derivative: The confidence region around the strong mean derivative almost goes down to zero and results in level-1 color coverage (cf. Fig. 3 (b)). Interestingly, the uncertainty in gradient orientation is almost unaffected in region (2). Thus, the orientation of the transition zone is stable, although the scalar standard deviation is quite high. For other prominent structures in the mean data in regions (3), (4) and (5), the glyphs indicate a strong orientation variability. Furthermore, the relatively low diffusion of the level-3 color and the strong presence of blue and red stripes indicate a high derivative uncertainty in region (3) (cf. Fig. 3 (d)).

In temperature forecasts, the proposed uncertainty visualizations help to identify regions where significant *and* stable temperature differences are present. This information allows adapting forecast probabilities of weather fronts with respect to the reliability of the respective features. Furthermore, it can be used to re-parameterize the numerical forecast simulations, for instance, to reduce or even eliminate the observed instabilities in the features. Such an analysis strives towards the use of uncertainty for sensitivity analysis, and, herewith, the tuning of simulation technologies towards more reliable and stable outputs.

6 CONCLUSION

In this work we presented two methods for visualizing the variability of gradients in 2D uncertain scalar fields: a color diffusion model for visualizing the derivative uncertainty and a glyph-based approach for visualizing the uncertainty in gradient orientation. At the core of these techniques are the probability distributions of the gradient magnitude and orientation, which we have derived in an analytic form in this paper. The proposed methods allow a quantitative analysis of the gradient variability, which is required for assessing the stability of geometric structures like iso-contours in the mean data field. Even though we showed that the derivation of uncertainty parameters and probability distributions can be extended to 3D, we focused exclusively on visualization techniques for 2D scalar fields.

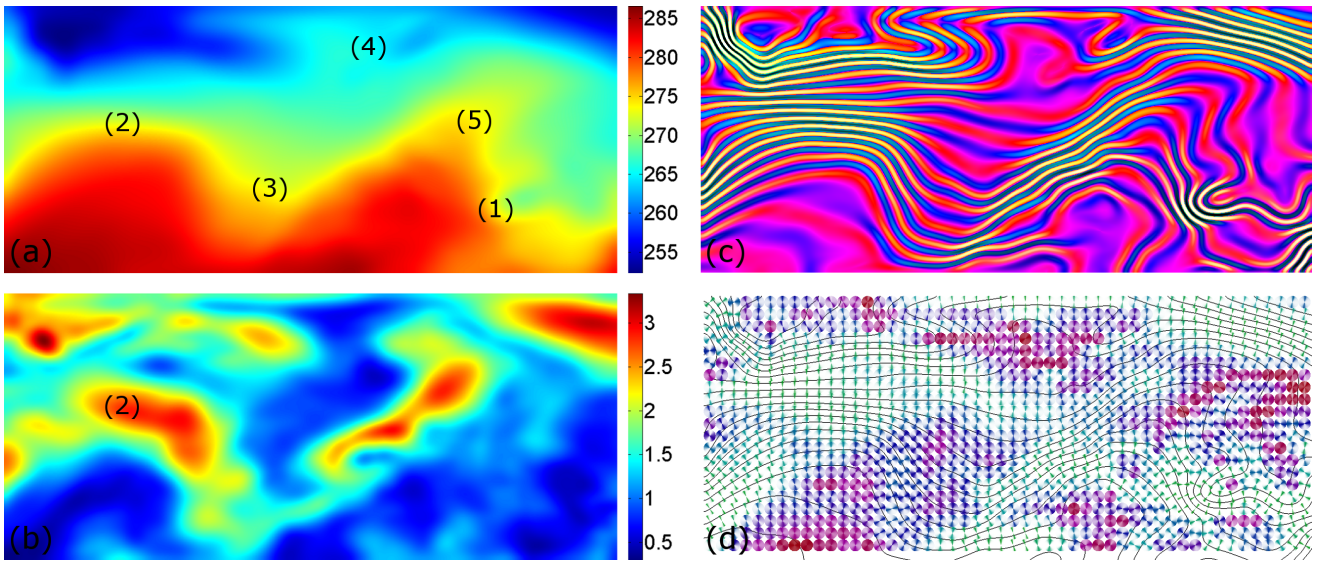


Fig. 10. Visualizations of mean values (a), standard deviations (b), derivative uncertainty (c), and orientation uncertainty (d) for an ensemble of temperature forecasts. A prominent structure with strong mean gradients and low uncertainty can be identified, for example, in (1). In (2), a strong standard deviation and therefore uncertainty in derivative is shown by the color diffusion over the black and white bands in (c). The green narrow glyphs in (d) indicate, nonetheless, that the derivative uncertainty does not affect the gradient orientation significantly. The orientation of the iso-lines is stable in (2), while in (3), (4), and (5), a significant variability in orientation and structure is emphasized.

In the future, one challenging endeavor will be the development of respective visualization techniques for 3D scalar fields. This, however, is difficult, because the proposed approaches cannot be transferred straightforwardly to 3D. For instance, the color diffusion technique for visualizing the derivative uncertainty cannot be embedded immediately into a volume rendering approach, since, due to blending and occlusions, the stripe pattern cannot be perceived anymore. An alternative approach would be to encode the derivative uncertainty via colors on a selected iso-surface. This, however, is dangerous, because it relates the derivative uncertainty to a specific iso-value, whereas our approaches strive for a visualization independent of the data value, but dependent on spatial positions.

To show the orientation uncertainty in 3D, we can simply map the 3D probability density values onto a sphere, and visualize the distributions via 3D spherical glyphs. This extension is demonstrated in Fig. 11 (b), where the distribution of the gradient orientation is mapped onto the unit sphere. Fig. 11 (a) shows the corresponding distribution parameters, with the mean represented by the magenta-colored vector and the covariance matrix by the yellow ellipsoid. The probability density is almost symmetric and bimodal. It can be observed that the direction given by the mean is rather unlikely.

Although the glyph-based approach for visualizing the orientation uncertainty can, in principle, be easily transferred to 3D, it introduces several specific problems: 3D glyphs have a spatial extent and occlude each other, severely limiting the number of glyphs that can be shown simultaneously. This problem could be addressed by showing glyphs only at particular spatial regions, but a specific interactive guidance functionality would then be required in order to draw the user’s attention to those interesting regions. Furthermore, the entire probability distribution encoded in one glyph cannot be seen from a specific viewpoint, because its “back-facing” part is always hidden. Ideally, a view-independent mapping of the entire spherical distribution would be required.

Although our proposed 2D visualization approaches have to be adapted to address the specific challenges in 3D, the mathematical foundations we laid out for modeling stochastically the variability of gradients in scalar fields are still valid, and can serve as fundamental basis for further research in this area.

ACKNOWLEDGMENTS

The work was partly funded by the European Union under the ERC Advanced Grant 291372: Safer-Vis - Uncertainty Visualization for Reliable Data Discovery.

APPENDIX A IRREGULAR GRID STRUCTURE

We assume an irregular grid structure $\mathbb{I}_m = \{\mathbf{x}_i : 1 \leq i \leq m\}$, where each grid point is connected to a set of neighboring grid points $N(\mathbf{x}_i)$ via edges. The data uncertainty at every point is modeled in exactly the same way as described in section 3. For a given point \mathbf{x}_i , the derivatives along the edges in the random field are approximated by one-sided differences, and they can also be expressed by the projection of the (unknown) gradient at \mathbf{x}_i onto the edges

$$\nabla Y(\mathbf{x}_i)^\top \frac{\mathbf{x}_j - \mathbf{x}_i}{\|\mathbf{x}_j - \mathbf{x}_i\|} = \frac{Y(\mathbf{x}_j) - Y(\mathbf{x}_i)}{\|\mathbf{x}_j - \mathbf{x}_i\|}, \quad \mathbf{x}_j \in N(\mathbf{x}_i). \quad (31)$$

For a vertex with n neighbors this can be written as a linear system

$$\mathbf{R}\nabla Y(\mathbf{x}_i) = \mathbf{b} \quad (32)$$

$$\mathbf{R} = [\mathbf{r}_1 | \mathbf{r}_2 | \dots | \mathbf{r}_n]^\top, \quad \mathbf{r}_j = \frac{\mathbf{x}_j - \mathbf{x}_i}{\|\mathbf{x}_j - \mathbf{x}_i\|} \quad (33)$$

$$b_j = \frac{Y(\mathbf{x}_j) - Y(\mathbf{x}_i)}{\|\mathbf{x}_j - \mathbf{x}_i\|} \quad (34)$$

Because in a d -dimensional grid the gradient has d components, d neighbors are required to solve for the gradient. However, as in a d -dimensional grid, every grid point has typically more than d

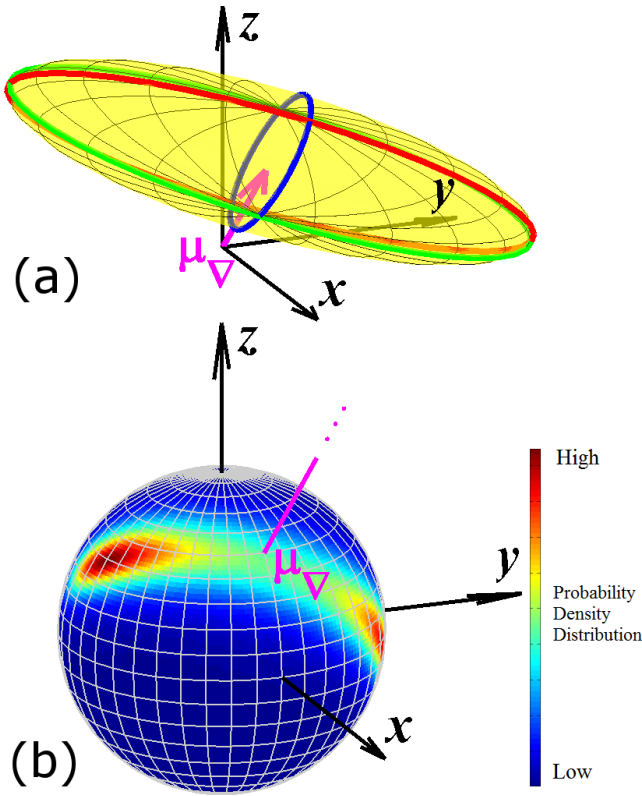


Fig. 11. (a) 3D Gaussian probability density of a gradient vector; The mean vector is drawn in magenta in the XZ-plane, and the tilted yellow ellipsoid indicates the confidence region. The three ellipses colored in red, green, and blue, respectively, are the corresponding ellipses having as semi-major and semi-minor axes the semi-axes of the ellipsoid. (b) The resulting bimodal probability density, mapped onto the unit sphere, where the magenta-colored line starting at the origin towards infinity has the direction of the mean vector.

neighbors, so that the system is over-determined, i.e., it is not guaranteed that a gradient exists that solves the equations for all neighbors. Thus, the system is solved using the least squares approach and the respective normal equation

$$\mathbf{R}^\top \mathbf{R} \nabla Y(\mathbf{x}_i) = \mathbf{R}^\top \mathbf{b} \quad (35)$$

$$\nabla Y(\mathbf{x}_i) = (\mathbf{R}^\top \mathbf{R})^{-1} \mathbf{R}^\top \mathbf{b} = \tilde{\mathbf{A}} \mathbf{b} \quad (36)$$

As the random variables at the grid points appear linearly in \mathbf{b} , and $\tilde{\mathbf{A}}$ is a linear operator, the mean vector and the covariance matrix for $\nabla Y(\mathbf{x}_i)$ can be obtained in more or less the same way as described in section 3.

APPENDIX B DERIVATION ORIENTATION UNCERTAINTY

To derive the formula for the distribution of the gradient direction in Equ. (10), we first express the θ -marginal by the integral of the product of a first order polynomial with an arbitrary Gaussian function

$$p_V^\theta(\theta) = C \int_0^\infty r \exp(-ar^2 + 2br + c) dr,$$

with variables

$$C = \frac{1}{2\pi \sqrt{\det \Sigma_V}}, \quad a = H(\cos \theta, \sin \theta), \quad b = t\sqrt{a}, \quad \text{and} \quad c = H(\mu_{\nabla_x}, \mu_{\nabla_y}),$$

and the auxiliary terms

$$H(x, y) = \frac{1}{2(1 - \rho_V^2)} \left(\frac{x^2}{\sigma_{\nabla_x}^2} + \frac{y^2}{\sigma_{\nabla_y}^2} - 2\rho_V \frac{xy}{\sigma_{\nabla_x} \sigma_{\nabla_y}} \right)$$

$$\text{and } t = \frac{-\mu_{\nabla_x} \sigma_{\nabla_y}^2 \cos \theta - \mu_{\nabla_y} \sigma_{\nabla_x}^2 \sin \theta}{2 \det \Sigma_V \sqrt{H(\cos \theta, \sin \theta)}} + \frac{\rho_V \sigma_{\nabla_x} \sigma_{\nabla_y} (\mu_{\nabla_x} \sin \theta + \mu_{\nabla_y} \cos \theta)}{2 \det \Sigma_V \sqrt{H(\cos \theta, \sin \theta)}}.$$

It follows that

$$p_V^\theta(\theta) = C \int_0^\infty r \exp(-ar^2 + 2br + c) dr =$$

$$= C \exp\left(\frac{b^2}{a} - c\right) \int_0^\infty r \exp\left(-\left(\sqrt{ar} + \frac{b}{\sqrt{a}}\right)^2\right) dr,$$

where the change of variables $\sqrt{ar} + b/\sqrt{a} = u$ gives

$$p_V^\theta(\theta) = \frac{C}{a} \exp\left(\frac{b^2}{a} - c\right) \int_{\frac{b}{\sqrt{a}}}^\infty \left(u - \frac{b}{\sqrt{a}}\right) \exp(-u^2) du =$$

$$= \frac{C}{2a} \exp\left(\frac{b^2}{a} - c\right) \left(\exp\left(-\frac{b^2}{a}\right) - \frac{2b}{\sqrt{a}} \int_{\frac{b}{\sqrt{a}}}^\infty \exp(-u^2) du \right) =$$

$$= \frac{C \exp(-c)}{2a} \left(1 - \sqrt{\pi} \frac{b}{\sqrt{a}} \exp\left(\frac{b^2}{a}\right) \left(1 - \operatorname{erf}\left(\frac{b}{\sqrt{a}}\right) \right) \right).$$

This can then be re-written to yield Equ. (10).

REFERENCES

- [1] C. Johnson and A. Sanderson, "A next step: Visualizing errors and uncertainty," *Computer Graphics and Applications, IEEE*, vol. 23, no. 5, pp. 6–10, 2003.
- [2] A. Pang, C. Wittenbrink, and S. Lodha, "Approaches to uncertainty visualization," *The Visual Computer*, vol. 13, no. 8, pp. 370–390, 1997.
- [3] T. Pfaffelmoser, M. Mihai, and R. Westermann, "Probability distributions for directions in gaussian distributed 3d scalar fields exemplified through gradients," Technische Universität München (http://www.cg.in.tum.de/fileadmin/user_upload/Lehrstuehle/Lehrstuhl_XV/Research/Publications/2012/Gradient_TechReport/TechnicalReport_Pfaffelmoser_20120827.pdf), Tech. Rep., 2012.
- [4] A. MacEachren, A. Robinson, S. Hopper, S. Gardner, R. Murray, M. Gahegan, and E. Hetzler, "Visualizing Geospatial Information Uncertainty: What We Know and What We Need to Know." *Cartography and Geographic Information Science*, vol. 32, no. 3, pp. 139–161, 2005.
- [5] A. Bostrom, L. Anselin, and J. Farris, "Visualizing Seismic Risk and Uncertainty," *Annals of the New York Academy of Sciences*, vol. 1128, no. 1, pp. 29–40, 2008.
- [6] H. Li, C. Fu, Y. Li, and A. Hanson, "Visualizing large-scale uncertainty in astrophysical data," *Visualization and Computer Graphics, IEEE Transactions on*, vol. 13, no. 6, pp. 1640–1647, 2007.
- [7] J. Thomson, E. Hetzler, A. MacEachren, M. Gahegan, and M. Pavel, "A typology for visualizing uncertainty," in *Proc. SPIE*, vol. 5669. Citeseer, 2005, pp. 146–157.
- [8] H. Griethel and H. Schumann, "The visualization of uncertain data: Methods and problems," in *Proceedings of SimVis 2006*, 2006, pp. 143–156.
- [9] K. Potter, <http://www.sci.utah.edu/~kpotter/library/uncertainVis/index.html>.
- [10] C. Wittenbrink, A. Pang, and S. Lodha, "Glyphs for visualizing uncertainty in vector fields," *Visualization and Computer Graphics, IEEE Transactions on*, vol. 2, no. 3, pp. 266–279, 2002.
- [11] S. Djurcilov, K. Kim, P. Lermusiaux, and A. Pang, "Visualizing scalar volumetric data with uncertainty," *Computers & Graphics*, vol. 26, no. 2, pp. 239–248, 2002.
- [12] P. Rhodes, R. Laramée, R. Bergeron, and T. Sparr, "Uncertainty visualization methods in isosurface rendering," in *Eurographics*. Citeseer, 2003, pp. 83–88.

- [13] C. Lundstrom, P. Ljung, A. Persson, and A. Ynnerman, "Uncertainty visualization in medical volume rendering using probabilistic animation," *Visualization and Computer Graphics, IEEE Transactions on*, vol. 13, no. 6, pp. 1648–1655, 2007.
- [14] J. Sanyal, S. Zhang, J. Dyer, A. Mercer, P. Amburn, and R. Moorhead, "Noodles: A Tool for Visualization of Numerical Weather Model Ensemble Uncertainty," *IEEE Transactions on Visualization and Computer Graphics*, 2010.
- [15] B. Zehner, N. Watanabe, and O. Kolditz, "Visualization of gridded scalar data with uncertainty in geosciences," *Computers & Geosciences*, 2010.
- [16] G. Kindlmann, R. Whitaker, T. Tasdizen, and T. Moller, "Curvature-based transfer functions for direct volume rendering: Methods and applications," in *Visualization, 2003. VIS 2003. IEEE*. IEEE, 2003, pp. 513–520.
- [17] G. Grigoryan and P. Rheingans, "Point-based probabilistic surfaces to show surface uncertainty," *Visualization and Computer Graphics, IEEE Transactions on*, vol. 10, no. 5, pp. 564–573, 2004.
- [18] R. Brown, "Animated visual vibrations as an uncertainty visualisation technique," in *GRAPHITE*. ACM, 2004, pp. 84–89.
- [19] T. Pfaffelmoser, M. Reitingner, and R. Westermann, "Visualizing the positional and geometrical variability of isosurfaces in uncertain scalar fields," in *Computer Graphics Forum*, vol. 30, no. 3. Wiley Online Library, 2011, pp. 951–960.
- [20] K. Pöthkow, B. Weber, and H. Hege, "Probabilistic marching cubes," in *Computer Graphics Forum*, vol. 30, no. 3. Wiley Online Library, 2011, pp. 931–940.
- [21] K. Pöthkow and H. Hege, "Positional uncertainty of isocontours: Condition analysis and probabilistic measures," *Visualization and Computer Graphics, IEEE Transactions on*, no. 99, pp. 1–1, 2010.
- [22] T. Pfaffelmoser and R. Westermann, "Visualization of global correlation structures in uncertain 2d scalar fields," in *Computer Graphics Forum*, vol. 31, no. 3pt2. Wiley Online Library, 2012, pp. 1025–1034.
- [23] —, "Correlation visualization for structural uncertainty analysis," *Int. J. Uncertain. Quantification*, 2012.
- [24] C. Yang, D. Xiu, and R. Kirby, "Visualization of covariance and cross-covariance fields," *International Journal for Uncertainty Quantification*, 2011.
- [25] C. Wittenbrink, A. Pang, and S. Lodha, "Glyphs for visualizing uncertainty in vector fields," *Visualization and Computer Graphics, IEEE Transactions on*, vol. 2, no. 3, pp. 266–279, 1996.
- [26] T. Zukab, J. Downtonb, D. Grayb, S. Carpendalea, and J. Liangb, "Exploration of uncertainty in bidirectional vector fields," 2008.
- [27] D. Jones, "Determining and visualizing uncertainty in estimates of fiber orientation from diffusion tensor mri," *Magnetic Resonance in Medicine*, vol. 49, no. 1, pp. 7–12, 2003.
- [28] A. Sanderson, C. Johnson, and R. Kirby, "Display of vector fields using a reaction-diffusion model," in *Visualization, 2004. IEEE*. IEEE, 2004, pp. 115–122.
- [29] R. Botchen, D. Weiskopf, and T. Ertl, "Texture-based visualization of uncertainty in flow fields," in *Visualization, 2005. VIS 05. IEEE*. Ieee, 2005, pp. 647–654.
- [30] R. Osorio and K. Brodlie, "Uncertain flow visualization using lic," *Proceedings of EG UK Theory and Practice of Computer Graphics*, pp. 1–9, 2009.
- [31] M. Otto, T. Germer, H. Hege, and H. Theisel, "Uncertain 2d vector field topology," in *Computer Graphics Forum*, vol. 29, no. 2. Wiley Online Library, 2010, pp. 347–356.
- [32] M. Otto, T. Germer, and H. Theisel, "Uncertain topology of 3d vector fields," in *Pacific Visualization Symposium (PacificVis), 2011 IEEE*. IEEE, 2011, pp. 67–74.
- [33] C. Petz, K. Pöthkow, and H. Hege, "Probabilistic local features in uncertain vector fields with spatial correlation," in *Computer Graphics Forum*, vol. 31, no. 3pt2. Wiley Online Library, 2012, pp. 1045–1054.
- [34] K. Mardia and P. Jupp, *Directional statistics*. Wiley, 2000, vol. 28, no. 1.
- [35] I. Mosca, L. Cobden, A. Deuss, J. Ritsema, and J. Trampert, "Seismic and mineralogical structures of the lower mantle from probabilistic tomography," *Journal of Geophysical Research*, vol. 117, no. B6, p. B06304, 2012.